Eur. Phys. J. Plus (2018) **133**: 133
DOI 10.1140/epjp/i2018-11954-7

THE EUROPEAN PHYSICAL JOURNAL PLUS

Regular Article

On the thermal buckling of magneto-electro-elastic piezoelectric nanobeams

Batoul Alibeigi[1], Yaghoub Tadi Beni[2,a], and Fahimeh Mehralian[1]

[1] Mechanical Engineering Department, Shahrekord University, Shahrekord, Iran
[2] Faculty of Engineering, Shahrekord University, Shahrekord, Iran

Received: 14 November 2017 / Revised: 22 February 2018
Published online: 30 March 2018 –

Abstract. In this paper, the buckling response of nanobeams on the basis of the Euler-Bernoulli beam model with the von Kármán geometrical nonlinearity using the modified couple stress theory is investigated under various types of thermal loading and electrical and magnetic fields. The modified couple stress theory, used in this paper, is capable to consider the higher-order electro-mechanical coupling effects besides size effects. The governing equations and boundary conditions are derived using minimum potential energy principle. The nanobeam is assumed to be under two types of thermal loading, uniform and linear, along thickness direction. The buckling response of nanobeams is studied using the Galerkin method and the effects of different parameters, such as size effect, length and thickness, on the critical buckling temperature are shown. The buckling behavior of nanobeam is illustrated significantly size-dependent particularly with an increase in thickness and decrease in length.

Introduction

Magneto-electro-thermo-elastic materials (METEMs), a specific category of smart materials, have attracted the attention of many researchers in recent years. These materials are able to generate electric and magnetic fields if stretched and they undergo deformation under magnetic and electrical loads. To date, many studies have been conducted on the physical and mechanical properties of METEMs [1]. In one study, Razavi and Shooshtari investigated the nonlinear free vibration of a symmetric rectangular electromagnetic elastic plate with simply supported boundary conditions. They developed the equations of motion using the first-order shear deformation theory and the von Kármán nonlinear strain and modeled the electric and magnetic behavior of the plate using Maxwell equations [2]. Liu *et al.* investigated the electro-thermo-mechanical free vibration of a nanoplate with simply supported boundary conditions using the nonlocal theory and the Kirchhoff theory and also demonstrating the effect of the nonlocal parameter, electric voltage, and temperature variation on the natural frequencies of the nanoplate [3].

Piezoelectric and piezomagnetic materials are used in engineering structures, particularly in sensors and actuators, for damping and controlling the vibrations. They are extensively used in microelectro-mechanical systems (MEMSs) and nanoelectro-mechanical systems (NEMSs) [4]. The distinctive capability of the materials in controlling deformation and delaying buckling has further increased the necessity of their investigation [5]. In this connection, Kumaravel *et al.* investigated the linear buckling and vibration of layered MEE beam subjected to uniform magnetic field using the finite element method under clamped conditions. They also examined the piezoelectric coupling effect on critical buckling magnetic field and vibration behavior [6].

In recent years, mechanical and electrical properties of piezoelectric and piezomagnetic materials have been investigated using laboratory techniques. Based on these investigations, researchers concluded that the mechanical and electrical properties of piezoelectric and piezomagnetic materials are size-dependent [7–13]. The classical continuum theory is efficient only in the analysis of macroscopic structures, and it fails to justify the size dependency of nanoelectro-mechanical systems [4]. Considering the shortcomings of classical continuum theories in incorporating size

[a] e-mail: tadi@eng.sku.ac.ir

effects, the higher-order continuum theories, which yield more accurate results by taking size effects into account, has been strongly recommended [14]. In this connection, due to the difficult nature of experiments at nano-scale and the time-consuming one of the molecular dynamics simulation, researchers have conducted many studies using higher-order continuum theories [15]. In this connection, Eringen introduced the nonlocal elasticity theory in order to take nano-scale effects into account in the classical continuum theory. According to this theory, stress at the reference point is a function of strain at other points within a certain domain [4]. In one study, Ke and Wang investigated thermo-electro-mechanical vibration of a piezoelectric nanobeam by using the Timoshenko beam model and by taking Eringen's nonlocal elasticity theory into consideration. They demonstrated the effects of temperature, nonlocal parameter, and input voltage on nanobeam vibration [16].

Other higher-order continuum theories including couple stress theory, strain gradient and shear deformation theory have been used by researchers to investigate size effects in micro and nano dimensions [17–21]. The couple stress theory was initially introduced by Toupin, Mindlin, Koiter and their colleagues as a nonclassical theory incorporating size effects [22–24]. This theory involves two extra material length scale parameters in order to describe the size effect of nano- and microstructures [25]. Anthoine studied the pure bending of circular cross-section beam based on the couple stress theory [26]. Due to the difficulty of computation of size effects of materials, Yang *et al.* developed the modified couple stress theory with a single size effect parameter. In this theory two material length scale parameters in the couple stress theory are decreased to one parameter [27]. Park and Gao analyzed bending of a Euler-Bernoulli beam based on a modified couple stress theory [28]. Reddy studied the static bending, free vibration and buckling problems of a simply supported beam using Euler-Bernoulli and Timoshenko models based on a modified couple stress theory and illustrated the effect of beam thickness parameter on deflection values [29].

Beams are structures with wide applications in MEMSs and NEMSs, and many studies have been conducted using these structural elements [4]. Beam models including the Euler-Bernoulli and the shear deformation models, that include the axial and transverse displacements and the angle of rotation of the cross-sections about vertical axis of any point on the mid-plane of the beam, respectively, have been widely used by researchers [30].

Also, Tadi Beni developed the nonlinear formulation of the isotropic piezoelectric Euler-Bernoulli beam on the basis of consistent size-dependent piezoelectricity. He investigated the vibration of a hinged nanobeam subjected to mechanical loads and drew a comparison between the results of linear and nonlinear classical vibration, and nonclassical vibration [31]. In one study, Tadi Beni studied the size-dependent electro-mechanical bending, buckling, and free vibration of a functionally graded piezoelectric nanobeam using Euler-Bernoulli model for clamped and cantilever boundary conditions. He demonstrated the effect of mechanical and electric load as well as the material properties of the functionally graded piezoelectric material on static responses, buckling, and free vibration [32].

When structures are exposed to thermal environments, thermal stress is created in the structures. As thermal stress reaches to certain level, the structures may lose their stability and undergo thermal buckling. Considering the exposure of many structures and nanostructures to thermal environments, it is highly necessary to investigate their behavior in such environments. In one study, Nateghi and Salamat-talab analyzed the thermal effect on buckling and free vibration of functionally graded microbeams using the modified couple stress theory and demonstrated the effect of temperature variation on size dependency [33]. Akgöz and Civalek investigated the thermo-mechanical buckling behavior of functionally graded microbeams using the modified couple stress theory and demonstrated the effect of size effects and length on the beam buckling behavior [34]. So far, few studies have been conducted on the thermal buckling of elastic piezoelectric and piezomagnetic nanobeams using higher-order theories.

In most previous studies, isotropic beams are assumed to be under uniform thermal loading and the buckling characteristics of only simply supported beam [34] in thermal environment are investigated [33,34]. Additionally, on the basis of the linear model, the critical buckling temperature, which leads to beam instability, are determined [33]. However, in the current study these limitations, by developing new formulation, are eliminated.

In the present paper, attempts are made for the first time to extract the nonlinear formulation of size-dependent thermal buckling of elastic piezoelectric and piezomagnetic nanobeams in a coupled fashion using the modified couple stress theory and Euler-Bernoulli beam model. In this study, the pre-buckling analysis has been presented as a fundamental and basic prerequisite for predicting the occurrence of buckling in the elastic piezoelectric and piezomagnetic nanobeam, and, afterwards, the analysis of thermal buckling of the nanobeam is carried out using the von Kármán nonlinear strain. Furthermore, the effects of geometrical parameters, boundary conditions, external electrical voltage and magnetic potential on the critical buckling temperature of the nanobeams are investigated.

It should be noted that the size effect has been taken into account in this formulation through using the modified couple stress theory for analysis the anisotropic nanostructures and can be used for isotropic ones as well. Besides, this formulation can turn into the classical beam formulation.

Note that there are many studies in which the piezoelectric and piezomagnetic nanobeams are investigated but only in this study the higher-order electro-mechanical coupling effect is considered. This is mainly due to the fact that the theory used in this paper is capable to consider the higher-order electro-mechanical coupling effect and that is more significant for beams with small scales.

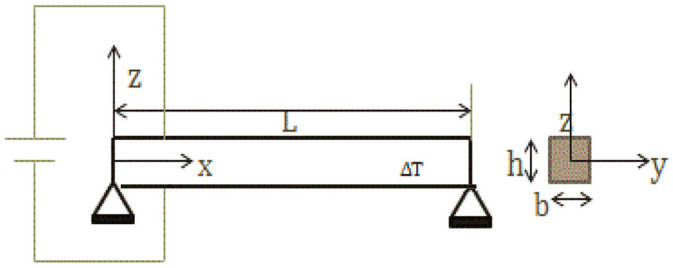

Fig. 1. Schematic view of the nanobeam.

Modified couple stress theory for piezoelectric materials

Based on the modified couple stress theory, which is able to incorporate the electro-mechanical coupling effect, the structural equations for a piezoelectric solid are expressed as [35,36]

$$\sigma_{ij} = c_{ijkl}\varepsilon_{kl} - e_{kij}E_k - q_{kij}H_k - \beta_{ij}\Delta T, \tag{1}$$

$$\tau_{ijk} = -f_{lijk}E_l + g_{ijklmn}\eta_{lmn}, \tag{2}$$

$$D_i = a_{ij}E_j + e_{ijk}\varepsilon_{jk} + d_{ij}H_j + f_{jkli}\eta_{jkl} + p_i\Delta T, \tag{3}$$

$$B_i = \mu_{ij}H_j + q_{ijk}\varepsilon_{jk} + d_{ij}E_j + \lambda_i\Delta T, \tag{4}$$

where B_i, D_i, σ_{ij}, τ_{ijk} represent the components of magnetic displacement, electric displacement, stress and higher-order stress, respectively; ΔT, β_{ij} stand for temperature change and thermal modulus, respectively; λ_i, p_i, μ_{ij}, d_{ij}, q_{ijk}, a_{ij}, e_{ijk}, c_{ijkl} represent pyromagnetic, pyroelectric, magnetic, electromagnetic, piezomagnetic, dielectric, piezoelectric, and elastic coefficients, respectively [35]; f_{lijk} is the electric field-strain gradient coupling coefficient tensors; g_{ijklmn} is strain gradient elasticity [36]. H_i, E_i, ε_{ij} stand for magnetic field, electric field, and strain, which are defined as follows:

$$\varepsilon_{ij} = \frac{1}{2}[u_{i,j} + u_{j,i} + u_{3,i}u_{3,j}], \tag{5}$$

$$E_k = -\frac{\partial\phi}{\partial x_i}, \qquad H_k = -\frac{\partial\psi}{\partial x_i}, \tag{6}$$

where ψ, ϕ stand for magnetic potential and electric potential, respectively, and u stands for displacement. The strain gradient tensor is expressed as

$$\eta_{ijk} = \varepsilon_{ij,k} = \frac{1}{2}[u_{i,jk} + u_{j,ik}], \tag{7}$$

where $\varepsilon_{ij} = \varepsilon_{ji}$, $\eta_{ijk} = \eta_{jik}$. If electro-mechanical coupling is not taken into account, all electric coefficients are set to zero. For centrosymmetric dielectric cases, coefficient e_{ijk} is set to zero [36].

In modified couple stress theory, used in this study, by setting strain gradient elasticity parameter, g_{ijklmn} and the electric field-strain gradient coupling coefficient tensors (the higher-order electro-mechanical coupling coefficient) f_{lijk} to zero, the formulation of classical continuum theory can be obtained.

Governing equations and related boundary conditions

A nanobeam of length L, width b, and height h is considered in fig. 1. The origin of the coordinate system is assumed to be on the beam's middle surface, such that the x-axis is along the beam's length and the z-axis is perpendicular to the beam's length.

Displacement at each point of nanobeam, based on the Euler-Bernoulli beam model, is expressed as [37]

$$u_1 = u_0(x) - z\frac{\partial w(x)}{\partial x}, \qquad u_2 = 0, \qquad u_3 = w(x). \tag{8}$$

The governing equation and boundary conditions are developed using the principle of minimum potential energy, according to the following equation:

$$\delta\Pi = \delta U - \delta W = 0, \tag{9}$$

where δW is the work variation of external loads acting on nanobeam, and δU is the variation of strain energy. According to the modified couple stress theory, the strain energy per volume for piezoelectric beams is determined as follows:

$$U = \frac{1}{2}\left[\sigma_{ij}(\varepsilon_{ij} - \alpha_{ij}\Delta T) + \tau_{ijk}\eta_{ijk} - D_k E_k - B_k H_k\right], \tag{10}$$

where α_{ij} represents thermal expansion coefficients. The relationship between thermal expansion coefficient and thermal modulus is expressed through the following equation [38], in which $\alpha_0 = \alpha_x$, Y_0 is meant for data normalization:

$$\beta_{xi} = \left(\frac{1}{\alpha_0 Y_0}\right)\left(c_{11i}\alpha_{xi} + c_{12i}\alpha_{yi} + c_{13i}\alpha_{zi}\right). \tag{11}$$

Components of the strain tensor and the strain gradient tensor are determined by substituting eq. (8) into eqs. (5) and (7) as follows:

$$\begin{aligned} \varepsilon_{xx} &= \frac{\partial u_0}{\partial x} - z\frac{\partial^2 w}{\partial x^2} + \frac{1}{2}\left(\frac{\partial w}{\partial x}\right)^2, \\ \eta_{xx} &= \frac{\partial^2 u_0}{\partial x^2} - z\frac{\partial^3 w}{\partial x^3}, \qquad \eta_{xz} = -\frac{\partial^2 w}{\partial x^2}. \end{aligned} \tag{12}$$

It should be noted that other components of the classical strain tensor and higher-order strain gradient tensor are equal to zero. By substituting eq. (12) into eqs. (1)–(4), the classical and higher-order stress as well as electric and magnetic displacements are determined as follows:

$$\sigma_{xx} = c_{1111}(\varepsilon_{xx} - \alpha_{11}\Delta T) - e_{311}E_z - q_{311}H_z, \tag{13}$$

$$\tau_{xx} = g_{111111}\eta_{xx}, \qquad \tau_{xz} = g_{113113}\eta_{xz} - f_{3113}E_z, \tag{14}$$

$$D_x = a_{11}E_x + d_{11}H_x + p_1\Delta T, \tag{15}$$

$$D_z = a_{33}E_z + d_{33}H_z + p_3\Delta T + e_{311}\varepsilon_{xx} + f_{3113}\eta_{xz}, \tag{16}$$

$$B_x = \mu_{11}H_x + d_{11}E_x + \lambda_1\Delta T, \tag{17}$$

$$B_z = \mu_{33}H_z + d_{33}E_z + \lambda_3\Delta T + q_{311}\varepsilon_{xx}. \tag{18}$$

The work of the external loads equals zero. Now, by substituting eqs. (12)–(18) into the strain energy equation and by using the calculus of variations, the following result is yielded:

$$\delta U = \int_0^L \int_A \left(\sigma_{xx}\delta(\varepsilon_{xx} - \alpha_{11}\Delta T) + \tau_{xx}\delta\eta_{xx} + \tau_{xz}\delta\eta_{xz} - D_x\delta E_x - D_z\delta E_z - B_x\delta H_x - B_z\delta H_z\right)\mathrm{d}A\mathrm{d}x, \tag{19}$$

$$\begin{aligned} \delta U = &\int_0^L \left(N\delta\left(\frac{\partial u_0}{\partial x} + \frac{1}{2}\left(\frac{\partial w}{\partial x}\right)^2\right) - M\delta\left(\frac{\partial^2 w}{\partial x^2}\right) + p\delta\left(\frac{\partial^2 u_0}{\partial x^2}\right) - M^H\delta\left(\frac{\partial^3 w}{\partial x^3}\right) - \overline{p}\delta\left(\frac{\partial^2 w}{\partial x^2}\right)\right)\mathrm{d}x \\ &+ \int_0^L \int_A \left(D_x\delta\left(\frac{\partial \phi}{\partial x}\right) + D_z\delta\left(\frac{\partial \phi}{\partial z}\right) + B_x\delta\left(\frac{\partial \psi}{\partial x}\right) + B_z\delta\left(\frac{\partial \psi}{\partial z}\right)\right)\mathrm{d}A\mathrm{d}x. \end{aligned} \tag{20}$$

In the latter equation, N is the axial force, M is the bending moment, M^H is the higher-order bending moment, and P is the summation of the axis couple stress on the cross-section:

$$N = \int_A \sigma_{xx}\mathrm{d}A, \qquad M = \int_A \sigma_{xx}z\mathrm{d}A, \qquad p = \int_A \tau_{xx}\mathrm{d}A, \qquad M^H = \int_A \tau_{xx}z\mathrm{d}A, \qquad \overline{p} = \int_A \tau_{xz}\mathrm{d}A. \tag{21}$$

Also, the governing equations are developed as follows:

$$\delta u_0 : \frac{\partial^2 p}{\partial x^2} - \frac{\partial N}{\partial x} = 0, \tag{22}$$

$$\delta w : \frac{\partial^3 M^H}{\partial x^3} - \frac{\partial^2 M}{\partial x^2} - \frac{\partial^2 \overline{p}}{\partial x^2} - \frac{\partial}{\partial x}\left(N\frac{\partial w}{\partial x}\right) = 0, \tag{23}$$

$$\delta \phi : \frac{\partial D_x}{\partial x} + \frac{\partial D_z}{\partial z} = 0, \tag{24}$$

$$\delta \psi : \frac{\partial B_x}{\partial x} + \frac{\partial B_z}{\partial z} = 0. \tag{25}$$

The boundary conditions are as follows:

$$\left(-\frac{\partial P}{\partial x}+N\right)\Big|_{x=0,L}=0,\quad \text{or}\quad \delta u_0\,|_{x=0,L}=0\ , \tag{26}$$

$$P\,|_{x=0,L}=0,\quad \text{or}\quad \delta\left(\frac{\partial u_0}{\partial x}\right)\Big|_{x=0,L}=0, \tag{27}$$

$$\left(-\frac{\partial^2 M^H}{\partial x^2}+\frac{\partial M}{\partial x}+\frac{\partial \overline{p}}{\partial x}+\left(N\frac{\partial w}{\partial x}\right)\right)\Big|_{x=0,L}=0,\quad \text{or}\quad \delta w\,|_{x=0,L}=0, \tag{28}$$

$$\left(\frac{\partial M^H}{\partial x}-M-\overline{p}\right)\Big|_{x=0,L}=0,\quad \text{or}\quad \delta\left(\frac{\partial w}{\partial x}\right)\Big|_{x=0,L}=0, \tag{29}$$

$$-M^H\,|_{x=0,L}=0,\quad \text{or}\quad \delta\left(\frac{\partial^2 w}{\partial x^2}\right)\Big|_{x=0,L}=0, \tag{30}$$

$$\int_{-\frac{h}{2}}^{\frac{h}{2}}(D_x)\,\mathrm{d}z\,|_{x=0,L}=0,\quad \text{or}\quad \delta\phi\,|_{x=0,L}=0, \tag{31}$$

$$\int_0^L(D_z)\,\mathrm{d}x\,\Big|_{z=-\frac{h}{2},\frac{h}{2}}=0,\quad \text{or}\quad \delta\phi\,\Big|_{z=-\frac{h}{2},\frac{h}{2}}=0, \tag{32}$$

$$\int_{-\frac{h}{2}}^{\frac{h}{2}}(B_x)\mathrm{d}z\,|_{x=0,L}=0,\quad \text{or}\quad \delta\psi\,|_{x=0,L}=0, \tag{33}$$

$$\int_0^L(B_z)\mathrm{d}x\,\Big|_{z=-\frac{h}{2},\frac{h}{2}}=0,\quad \text{or}\quad \delta\psi\,\Big|_{z=-\frac{h}{2},\frac{h}{2}}=0. \tag{34}$$

By substituting eq. (12) and eqs. (13)–(18) into the governing equations and boundary conditions, all the equations are developed as follows:

$$Ag_{111111}\frac{\partial^4 u_0}{\partial x^4}-Ac_{1111}\left(\frac{\partial^2 u_0}{\partial x^2}+\frac{1}{2}\frac{\partial}{\partial x}\left(\frac{\partial w}{\partial x}\right)^2\right)-be_{311}\frac{\partial}{\partial x}\left(\int_{-\frac{h}{2}}^{\frac{h}{2}}\frac{\partial\phi}{\partial z}\mathrm{d}z\right)-bq_{311}\frac{\partial}{\partial x}\left(\int_{-\frac{h}{2}}^{\frac{h}{2}}\frac{\partial\psi}{\partial z}\mathrm{d}z\right)=0, \tag{35}$$

$$\begin{aligned}&-Ig_{111111}\frac{\partial^6 w}{\partial x^6}+Ic_{1111}\frac{\partial^4 w}{\partial x^4}+Ag_{113113}\frac{\partial^4 w}{\partial x^4}-bf_{3113}\frac{\partial^2}{\partial x^2}\left(\int_{-\frac{h}{2}}^{\frac{h}{2}}\frac{\partial\phi}{\partial z}\mathrm{d}z\right)-\left(\frac{\partial w}{\partial x}\right)\left[Ac_{1111}\left(\frac{\partial^2 u_0}{\partial x^2}+\frac{1}{2}\frac{\partial}{\partial x}\left(\frac{\partial w}{\partial x}\right)^2\right)\right.\\&\left.+be_{311}\frac{\partial}{\partial x}\left(\int_{-\frac{h}{2}}^{\frac{h}{2}}\frac{\partial\phi}{\partial z}\mathrm{d}z\right)+bq_{311}\frac{\partial}{\partial x}\left(\int_{-\frac{h}{2}}^{\frac{h}{2}}\frac{\partial\psi}{\partial z}\mathrm{d}z\right)\right]-\left(\frac{\partial^2 w}{\partial x^2}\right)\left[Ac_{1111}\left(\frac{\partial u_0}{\partial x}+\frac{1}{2}\left(\frac{\partial w}{\partial x}\right)^2\right)\right.\\&\left.+be_{311}\left(\int_{-\frac{h}{2}}^{\frac{h}{2}}\frac{\partial\phi}{\partial z}\mathrm{d}z\right)+bq_{311}\left(\int_{-\frac{h}{2}}^{\frac{h}{2}}\frac{\partial\psi}{\partial z}\mathrm{d}z\right)-N_x^T\right]=0,\end{aligned} \tag{36}$$

$$a_{11}\frac{\partial^2\phi}{\partial x^2}+d_{11}\frac{\partial^2\psi}{\partial x^2}+a_{33}\frac{\partial^2\phi}{\partial z^2}+d_{33}\frac{\partial^2\psi}{\partial z^2}+e_{311}\frac{\partial^2 w}{\partial x^2}-p_3\frac{\partial}{\partial z}(\Delta T)=0, \tag{37}$$

$$\mu_{11}\frac{\partial^2\psi}{\partial x^2}+d_{11}\frac{\partial^2\phi}{\partial x^2}+\mu_{33}\frac{\partial^2\psi}{\partial z^2}+d_{33}\frac{\partial^2\phi}{\partial z^2}+q_{311}\frac{\partial^2 w}{\partial x^2}-\lambda_3\frac{\partial}{\partial z}(\Delta T)=0. \tag{38}$$

The boundary conditions are as follows:

$$\left(-Ag_{111111}\frac{\partial^3 u_0}{\partial x^3}+Ac_{1111}\left(\frac{\partial u_0}{\partial x}+\frac{1}{2}\left(\frac{\partial w}{\partial x}\right)^2\right)+be_{311}\left(\int_{-\frac{h}{2}}^{\frac{h}{2}}\frac{\partial\phi}{\partial z}\mathrm{d}z\right)+bq_{311}\left(\int_{-\frac{h}{2}}^{\frac{h}{2}}\frac{\partial\psi}{\partial z}\mathrm{d}z\right)-N_x^T\right)\Big|_{x=0,L}=0,$$
$$\text{or}\quad \delta u_0|_{x=0,L}=0, \tag{39}$$

$$\left(Ag_{111111}\frac{\partial^2 u_0}{\partial x^2}\right)\Big|_{x=0,L}=0,\quad \text{or}\quad \delta\left(\frac{\partial u_0}{\partial x}\right)\Big|_{x=0,L}=0, \tag{40}$$

$$\left(Ig_{111111}\frac{\partial^5 w}{\partial x^5}-Ic_{1111}\frac{\partial^3 w}{\partial x^3}-Ag_{113113}\frac{\partial^3 w}{\partial x^3}+bf_{3113}\frac{\partial}{\partial x}\left(\int_{-\frac{h}{2}}^{\frac{h}{2}}\frac{\partial\phi}{\partial z}\mathrm{d}z\right)+\left(\frac{\partial w}{\partial x}\right)\left(Ac_{1111}\left(\frac{\partial u_0}{\partial x}+\frac{1}{2}\left(\frac{\partial w}{\partial x}\right)^2\right)\right.\right.$$
$$\left.\left.+be_{311}\left(\int_{-\frac{h}{2}}^{\frac{h}{2}}\frac{\partial\phi}{\partial z}\mathrm{d}z\right)+bq_{311}\left(\int_{-\frac{h}{2}}^{\frac{h}{2}}\frac{\partial\psi}{\partial z}\mathrm{d}z\right)-N_x^T\right)\right)\Bigg|_{x=0,L}=0,\quad \text{or}\quad \delta w\,|_{x=0,L}=0, \tag{41}$$

$$\left(-Ig_{111111}\frac{\partial^4 w}{\partial x^4}+Ic_{1111}\frac{\partial^2 w}{\partial x^2}-bf_{3113}\left(\int_{-\frac{h}{2}}^{\frac{h}{2}}\frac{\partial\phi}{\partial z}\mathrm{d}z\right)+Ag_{13113}\frac{\partial^2 w}{\partial x^2}+M_x^T\right)\Bigg|_{x=0,L}=0,\quad \text{or}\quad \delta\left(\frac{\partial w}{\partial x}\right)|_{x=0,L}=0, \tag{42}$$

$$Ig_{111111}\frac{\partial^3 w}{\partial x^3}\Bigg|_{x=0,L}=0,\quad \text{or}\quad \delta\left(\frac{\partial^2 w}{\partial x^2}\right)\Bigg|_{x=0,L}=0, \tag{43}$$

$$\int_{-\frac{h}{2}}^{\frac{h}{2}}\left(-a_{11}\frac{\partial\phi}{\partial x}-d_{11}\frac{\partial\psi}{\partial x}+p_1\Delta T\right)\mathrm{d}z\Bigg|_{x=0,L}=0,\quad \text{or}\quad \delta\phi|_{x=0,L}=0, \tag{44}$$

$$\int_0^L\left(-a_{33}\frac{\partial\phi}{\partial z}-d_{33}\frac{\partial\psi}{\partial z}+e_{311}\left(\frac{\partial u_0}{\partial x}-z\frac{\partial^2 w}{\partial x^2}+\frac{1}{2}\left(\frac{\partial w}{\partial x}\right)^2\right)+p_3\Delta T-f_{3113}\left(\frac{\partial^2 w}{\partial x^2}\right)\right)\mathrm{d}x\Bigg|_{z=-\frac{h}{2},\frac{h}{2}}=0,$$

$$\text{or}\quad \delta\phi\,\Big|_{z=-\frac{h}{2},\frac{h}{2}}=0, \tag{45}$$

$$\int_{-\frac{h}{2}}^{\frac{h}{2}}\left(-\mu_{11}\frac{\partial\psi}{\partial x}-d_{11}\frac{\partial\phi}{\partial x}+\lambda_1\Delta T\right)\Bigg|_{x=0,L}\mathrm{d}z=0,\quad \text{or}\quad \delta\psi|_{x=0,L}=0, \tag{46}$$

$$\int_0^L\left(-d_{33}\frac{\partial\phi}{\partial z}-\mu_{33}\frac{\partial\psi}{\partial z}+q_{311}\left(\frac{\partial u_0}{\partial x}-z\frac{\partial^2 w}{\partial x^2}+\frac{1}{2}\left(\frac{\partial w}{\partial x}\right)^2\right)+\lambda_3\Delta T\right)\mathrm{d}x\Bigg|_{z=-\frac{h}{2},\frac{h}{2}}=0,\qquad \text{or}\qquad \delta\psi\,\Big|_{z=-\frac{h}{2},\frac{h}{2}}=0. \tag{47}$$

Note that the open circuit boundary conditions (45) and (47) are as follows:

$$\int_0^L\left(-a_{33}\frac{\partial\phi}{\partial z}-d_{33}\frac{\partial\psi}{\partial z}+e_{311}\left(\frac{\partial u_0}{\partial x}-z\frac{\partial^2 w}{\partial x^2}+\frac{1}{2}\left(\frac{\partial w}{\partial x}\right)^2\right)+p_3\Delta T-f_{3113}\left(\frac{\partial^2 w}{\partial x^2}\right)\right)\mathrm{d}x\Bigg|_{z=-\frac{h}{2},\frac{h}{2}}=0,$$

$$\int_0^L\left(-d_{33}\frac{\partial\phi}{\partial z}-\mu_{33}\frac{\partial\psi}{\partial z}+q_{311}\left(\frac{\partial u_0}{\partial x}-z\frac{\partial^2 w}{\partial x^2}+\frac{1}{2}\left(\frac{\partial w}{\partial x}\right)^2\right)+\lambda_3\Delta T\right)\mathrm{d}x\Bigg|_{z=-\frac{h}{2},\frac{h}{2}}=0.$$

In the above equations, I, A represent area moment of inertia of sections about the y-axis and cross-section, respectively. Also, N_x^T and M_x^T are thermal moment and thermal force resultants, respectively, which are expressed as follows:

$$N_x^T=\int_A\left(c_{1111}\alpha_{11}\Delta T\right)\mathrm{d}z,\qquad M_x^T=\int_A\left(c_{1111}\alpha_{11}\Delta T\right)z\mathrm{d}z. \tag{48}$$

Types of thermal distributions

Uniform temperature rise (UTR)

For nanobeams made of isotropic and anisotropic materials at reference temperature T_0, uniform temperature rise in all points will reach the ultimate value T. Therefore, temperature variation among all points of the nanobeams is expressed as

$$\Delta T=T-T_0. \tag{49}$$

Linear temperature rise (LTR)

For nanobeams made of isotropic materials whose thickness is assumed to be thin enough, approximate temperature rise along nanobeam thickness varies linearly,

$$T = T_1 + \Delta T\left(\frac{1}{2} + \frac{z}{h}\right), \tag{50}$$

where $\Delta T = T_2 - T_1$ is temperature difference, where T_1 is the lower temperature of nanobeam and T_2 is the upper ones.

Pre-buckling deformation

This investigation attempts an analysis of the buckling of fully flat nanobeams. For this purpose, the deformation of the piezoelectric and piezomagnetic nanobeams must be examined so as to ensure that the nanobeams remain flat under transverse thermal load [39]. In the investigation of pre-buckling deformation, assuming that the equations are linear and that nanobeam deformation prior to buckling equals zero ($w^p(x) = 0$). Hence, by setting $w^p(x) = 0$ in the governing equations (35)–(38), an equilibrium position in the pre-buckling state follows the equations:

$$\begin{aligned}
&Ag_{111111}\frac{\partial^4 u_0}{\partial x^4} - Ac_{1111}\left(\frac{\partial^2 u_0}{\partial x^2}\right) - be_{311}\frac{\partial}{\partial x}\left(\int_{-\frac{h}{2}}^{\frac{h}{2}}\frac{\partial \varphi}{\partial z}\mathrm{d}z\right) - bq_{311}\frac{\partial}{\partial x}\left(\int_{-\frac{h}{2}}^{\frac{h}{2}}\frac{\partial \psi}{\partial z}\mathrm{d}z\right) = 0,\\
&bf_{3113}\frac{\partial^2}{\partial x^2}\left(\int_{-\frac{h}{2}}^{\frac{h}{2}}\frac{\partial \varphi}{\partial z}\mathrm{d}z\right) = 0,\\
&a_{11}\frac{\partial^2 \varphi}{\partial x^2} + d_{11}\frac{\partial^2 \psi}{\partial x^2} + a_{33}\frac{\partial^2 \varphi}{\partial z^2} + d_{33}\frac{\partial^2 \psi}{\partial z^2} = 0,\\
&\mu_{11}\frac{\partial^2 \psi}{\partial x^2} + d_{11}\frac{\partial^2 \varphi}{\partial x^2} + \mu_{33}\frac{\partial^2 \psi}{\partial z^2} + d_{33}\frac{\partial^2 \varphi}{\partial z^2} = 0.
\end{aligned} \tag{51}$$

Now, if the above equations in different boundary conditions (simply supported and clamped) are satisfied, the bifurcation-type buckling exists because, under such conditions, the beam remains flat prior to buckling. To do this, first, by solving the third and fourth relations of eq. (51), the electric potential and magnetic potential function are obtained as

$$\begin{aligned}
\varphi(x,z) &= \sum_{n=1}^{\infty}\left(\left(C_n\sinh\left(\frac{n\pi}{L}z\right) + D_n\cosh\left(\frac{n\pi}{L}z\right)\right)\sin\left(\frac{n\pi}{L}x\right)\right),\\
\psi(x,z) &= \sum_{n=1}^{\infty}\left(\left(E_n\sinh\left(\frac{n\pi}{L}z\right) + F_n\cosh\left(\frac{n\pi}{L}z\right)\right)\sin\left(\frac{n\pi}{L}x\right)\right),
\end{aligned} \tag{52}$$

where C_n, D_n, E_n, F_n are constant coefficients. Given the necessity of satisfying eq. (36), on the assumption of $(w^p(x) = 0)$, it is clear that the electric potential field above and below the nanobeam must be set to zero (open circuit condition). In other words, C_n, D_n, E_n, F_n are zero, and the second to fourth relations in eq. (52) are established. Now, by solving first relation in eq. (51), the nanobeam axial displacement equation is determined as follows:

$$\begin{aligned}
&Ag_{111111}\left(\frac{\partial^4 u_0}{\partial x^4}\right) - Ac_{1111}\left(\frac{\partial^2 u_0}{\partial x^2}\right) = 0,\\
&u_0(x) = C_1 + C_2 x + C_3 e^{\lambda x} + C_4 e^{-\lambda x},\\
&\lambda = \sqrt{\frac{c_{1111}}{g_{111111}}},
\end{aligned} \tag{53}$$

where C_4, C_3, C_2, C_1 are constant coefficients. By applying the boundary conditions of the nanobeam as $(u_0(x)|_{x=0} = u_0(x)|_{x=L} = (\frac{\partial^2 u_0(x)}{\partial x^2})|_{x=0,L} = 0)$ and by calculating the constant coefficients, the axial displacement of the nanobeam is determined. It should be noted that, although the beam has an axial displacement but the transvers displacement of beam is zero and the beam remains flat prior to buckling.

By determining axial displacement as well as electric and magnetic fields of the nanobeam, and by assuming that nanobeam deflection prior to buckling is zero (on the assumption of uniform temperature rise for the simply supported nanobeam and uniform and linear rise for the clamped nanobeam), all governing equations and boundary conditions are satisfied in eq. (51).

Therefore, the assumed nanobeam remains flat under transverse thermal load and continues bifurcating buckling.

Buckling analysis

Many methods can be used to determine the elastic critical load of the beams. It should be noted that the main method is based on the stability equations and solve the eigenvalue problem accordingly. But, here we used two methods: 1) analytical method and 2) stability equations.

In the first method, the governing equations are solved and the deflection of beam is obtained. Therefore, by increasing incrementally the applied temperature, and by detecting the large and sudden change of the deflection of beam, critical buckling temperature can be obtained.

In the second method, the stability equations obtained and then the eigenvalue problem solve according to the boundary conditions.

It should be noted that, to show the accuracy of the analytical method, the results of the analytical method and stability equations are compared and can be seen there is good consistency between the results of the two methods.

It should be noted that, in the analytical method, the formulation of the nanobeam has been developed for anisotropic materials and therefore the anisotropic beam can be investigated through this formulation. Note that this formulation can be used for isotropic beams as well. Also, on the basis of the nonlinear model, which leads to more realistic modeling of nanostructures, one can model more precisely many elements used in nanostructures, like nanobeames.

Analytical method

Analysis of nanobeam made of isotropic materials

In order to analyse the buckling of nanotubes made of isotropic materials, as the first step, all piezoelectric and piezomagnetic coefficients (e_{311} and q_{311}) are set equal to zero. Afterwards, given the difficulty of simultaneous solution of all the four differential couple equations, the semi-analytic Galerkin method is used. Hence, by solving eqs. (37) and (38) as two-dimensional Laplace equations, and by considering boundary conditions (44) and (46) ($\phi|_{x=o,L} = 0, \psi|_{x=0,L} = 0$) the electric and magnetic fields are determined as follows:

$$\phi(x,z) = A_k \sin\left(\frac{\pi}{L}x\right)\sinh\left(\frac{\pi}{L}z\right),$$
$$\psi(x,z) = B_k \sin\left(\frac{\pi}{L}x\right)\sinh\left(\frac{\pi}{L}z\right). \tag{54}$$

Coefficients A_k and B_k are determined using open circuit boundary conditions,

$$A_k = \left(\frac{1}{X_1}\right)\left(\left(\frac{d_{33}}{\mu_{33}}\right)(\lambda_3 \Delta T L) - 2f_{3113}\left(\frac{a\pi}{L}\right) - p_3 \Delta T L\right),$$
$$B_k = \left(\frac{1}{\mu_{33}}\right)\left(-d_{33}A_k + \frac{\lambda_3 \Delta T L}{2\cosh\left(\frac{\pi h}{2L}\right)}\right). \tag{55}$$

Given the assumption of hinged conditions, the nanobeam deflection function is as follows:

$$w(x) = \sum_{n=1}^{\infty} a \sin\left(\frac{n\pi}{L}x\right). \tag{56}$$

The nanobeam deflection function should satisfy the hinged boundary conditions as

$$w\,|_{x=0,L} = 0, \qquad \left(-Ig_{111111}\frac{\partial^4 w}{\partial x^4} + Ic_{1111}\frac{\partial^2 w}{\partial x^2} - bf_{3113}\left(\int_{-\frac{h}{2}}^{\frac{h}{2}}\frac{\partial \phi}{\partial z}\mathrm{d}z\right) + Ag_{113113}\frac{\partial^2 w}{\partial x^2}\right)\Bigg|_{x=0,L} = 0,$$
$$\left(\frac{\partial^2 w}{\partial x^2}\right)\Bigg|_{x=0,L} = 0,$$

where a is the nanobeam deflection amplitude and the assumption $n = 1$ has been made. By considering the nanobeam deflection function in the format of the forgoing equation, nanobeam axial displacement $u_0(x)$ is determined through eq. (35), and constant coefficients are computed using boundary conditions as $(u_0(x)|_{x=0,L} = 0, (\frac{\partial^2 u_0(x)}{\partial x^2})|_{x=0,L} = 0)$

$$u(x) = C_1 e^{\lambda_1 x} + C_2 e^{-\lambda_1 x} + C_3 x + \lambda_2 \sin\left(\frac{2\pi}{L}x\right) + C_4,$$
$$\lambda_1 = \sqrt{\frac{c_{1111}}{g_{111111}}}, \qquad \lambda_2 = -\lambda_1^2 \left(\frac{a^2 \pi L}{8\left(L^2 + 4(\frac{\pi}{\lambda_1})^2\right)}\right). \tag{57}$$

Now, by substituting eqs. (54), (56) and (57) in eq. (36), which is known as the beam deflection equation, this equation becomes based upon parameter (a) or nanobeam deflection amplitude (see eq. (58)). In this equation, the critical beam temperature which is assumed to be uniform along beam thickness, is unknown. By computing beam deflection amplitude through the equation below, the critical buckling temperature, which leads to nanobeam instability, can be determined:

$$Y_0 a^3 + Y_1 a + Y_2 = 0,$$
$$Y_0 = \left(\frac{Ac_{11111}}{2}\right)^2 \left(\frac{\pi}{L}\right)^3 \left(\left(\left(\frac{-X_2}{4AX_3}\right)\left(1 + \frac{X_2 L}{2\pi}\right) - \left(\frac{1}{X_4}\right)^2 \left(\frac{\pi}{4AX_3 L}\right)\left(1 - \left(\frac{X_2 L}{2\pi}\right)^2\right)\right)\left(\frac{2(\cosh(X_4 L) - 1)^2}{\sinh(X_4 L)}\right)\right.$$
$$\left. + \left(\frac{2}{Ac_{1111}}\right)\left(\frac{\pi}{L}\right)\left(\frac{\pi}{4} + \frac{L}{8}\right)\right),$$
$$Y_1 = \left(\frac{L}{2}\right)\left(\frac{\pi}{L}\right)^4 \left(-\frac{2{f^2}_{3113}\sinh\left(\frac{\pi h}{2L}\right)}{\left(\frac{\pi}{L}\right)X_1} + Ig_{111111}\left(\frac{\pi}{L}\right)^2 + Ic_{1111} + Ag_{113113}\right),$$
$$+ (Ac_{11111})\left(\frac{\pi}{L}\right)(N_x^T)\left(\left(\frac{X_2}{4AX_3}\right) + \left(\frac{1}{X_4}\right)^2 \left(\frac{\pi}{L}\right)\left(\frac{1}{4AX_3}\right)\left(1 - \frac{X_2 L}{2\pi}\right)\right)\left(\frac{2\left(1 - \cosh(X_4 L)\right)^2}{\sinh(X_4 L)}\right),$$
$$Y_2 = f_{3113}\left(\frac{\pi}{L}\right)^2 \left(\frac{L}{2}\right)\sinh\left(\frac{\pi h}{2L}\right)\left(\frac{\left(\frac{d_{33}}{\mu_{33}}\right)(\lambda_3 \Delta T L) - (p_3 \Delta T L)}{2X_1}\right),$$
$$X_1 = 2\cosh\left(\frac{\pi h}{2L}\right)\left(-a_{33} + \frac{{d_{33}}^2}{\mu_{33}}\right), \qquad X_2 = \frac{\left(\frac{L}{2\pi}\right)}{1 + \left(\frac{1}{X_4}\right)^2 \left(\frac{L}{2\pi}\right)^2}, \qquad X_3 = (c_{1111} g_{111111})^{\frac{1}{2}},$$
$$X_4 = \left(\frac{c_{1111}}{g_{111111}}\right)^{\frac{1}{2}}. \tag{58}$$

In order to investigate clamped nanobeams, the nanobeam deflection function is formulated as in the following format:

$$w(x) = \sum_{n=1}^{\infty} a \sin^2\left(\frac{n\pi}{L}x\right) \tag{59}$$

and clamped boundary condition is as

$$w\,|_{x=0,L} = 0, \qquad \left(\frac{\partial w}{\partial x}\right)\Big|_{x=0,L} = 0, \qquad \left(\frac{\partial^3 w}{\partial x^3}\right)\Big|_{x=0,L.} = 0.$$

So the previous procedure should be repeated on eq. (36), and the critical buckling temperature can be obtained in similar way. Note that in this boundary condition temperature distribution is considered uniform and linear.

Analysis of nanobeam made of anisotropic materials

In order to analysis the buckling of anisotropic nanobeam, the Galerkin method is utilized and the nanobeam deflection function is assumed according to eq. (56). Also by solving eqs. (37) and (38) and considering boundary conditions

as $(\phi|_{x=o,L}=0,\psi|_{x=0,L}=0)$, the electric potential field and magnetic potential field on the assumption of uniform temperature are obtained as follows:

$$\begin{aligned}
\phi(x,z) &= A_k X_2' \sin\left(\frac{\pi}{L}x\right)\left(1-\sin\left(X_1'\frac{\pi}{L}z\right)\right),\\
\psi(x,z) &= B_k X_{22} \sin\left(\frac{\pi}{L}x\right)\left(1-\sin\left(X_{11}\frac{\pi}{L}z\right)\right),\\
X_1' &= \left(\frac{a_{11}-d_{11}}{a_{33}-d_{33}}\right), \quad X_2' = a\left(\frac{q_{311}-e_{311}}{a_{11}-d_{11}}\right), \qquad X_{11} = \left(\frac{d_{11}-\mu_{11}}{d_{33}-\mu_{33}}\right), \qquad X_{22} = a\left(\frac{q_{311}-e_{311}}{d_{11}-\mu_{11}}\right).
\end{aligned} \tag{60}$$

Coefficients A_k and B_k are determined using open circuit boundary conditions:

$$\begin{aligned}
A_k &= \left(\left(\frac{1}{8}\right)\frac{\left((\pi a)^2+4\pi a h\right)\left(d_3 q_{311}-e_{311}\mu_3\right)+4L^2\Delta T\left(d_3\lambda_3-p_3\mu_3\right)-8\pi a f_{3113}\mu_{33}}{LX_1'X_2'\cos\left(\frac{\pi h X_1'}{2L}\right)\left(a_3\mu_3-d_3^2\right)}\right),\\
B_k &= \left(\left(-\frac{1}{8}\right)\frac{A_k d_{33}\left(LX_1'X_2'\cos\left(\frac{\pi h X_1'}{2L}\right)\right)+\left((\pi a)^2+4\pi a h\right)q_{311}+4L^2\Delta T\lambda_3}{LX_{11}X_{22}\mu_{33}\cos\left(\frac{\pi h X_{11}}{2L}\right)}\right).
\end{aligned} \tag{61}$$

Thus, by considering eqs. (56) and (60), the axial nanobeam displacement $u_0(x)$ can be computed using eq. (35) and boundary conditions as $(u_0(x)|_{x=0,L}=0,(\frac{\partial^2 u_0(x)}{\partial x^2})|_{x=0,L}=0)$. Also, by substituting beam deflection function, axial nanobeam displacement, and electric and magnetic potential functions into eq. (36), this equation is developed as an equation based upon parameter (a) and critical buckling temperature can be obtained as before. It should be noted that uniform temperature distribution is considered here.

Stability equations

To obtain the stability equations, the adjacent equilibrium criterion is utilized. The small increments to the displacement variables have been given in order to investigate the possible existence of adjacent equilibrium configurations. Afterwards, the two adjacent configurations indicated by displacements before and after increment are investigated [10, 40]. Thus

$$\begin{aligned}
u_0 &= U_0 + U_1,\\
w &= W_0 + W_1,
\end{aligned} \tag{62}$$

where U_0 and W_0 are displacement components of the equilibrium state and U_1 and W_1 are arbitrary small increment.

Similar to eq. (62), the electric potential and magnetic potential are found to be the sum of those related to the equilibrium and neighboring states as

$$\begin{aligned}
\varphi &= \varphi_0 + \varphi_1,\\
\psi &= \psi_0 + \psi_1.
\end{aligned} \tag{63}$$

By substituting eqs. (62) and (63) into eqs. (35)–(38), the stability equations are obtained. It should be noted that the terms U_0, W_0, ϕ_0, ψ_0 satisfy the equilibrium conditions and drop out and the nonlinear terms with subscript 1 are small in comparison to the linear terms, therefore this terms are ignored. The stability equations are obtained as

$$Ag_{111111}\frac{\partial^4 U_1}{\partial x^4} - Ac_{1111}\left(\frac{\partial^2 U_1}{\partial x^2}\right) = 0, \tag{64}$$

$$-Ig_{111111}\frac{\partial^6 W_1}{\partial x^6} + Ic_{1111}\frac{\partial^4 W_1}{\partial x^4} + Ag_{113113}\frac{\partial^4 W_1}{\partial x^4} - N_x'\frac{\partial^2 W_1}{\partial x^2} = 0, \tag{65}$$

$$a_{11}\frac{\partial^2\varphi_1}{\partial x^2} + d_{11}\frac{\partial^2\psi_1}{\partial x^2} + a_{33}\frac{\partial^2\varphi_1}{\partial z^2} + d_{33}\frac{\partial^2\psi_1}{\partial z^2} + e_{311}\frac{\partial^2 W_1}{\partial x^2} = 0, \tag{66}$$

$$\mu_{11}\frac{\partial^2\psi_1}{\partial x^2} + d_{11}\frac{\partial^2\varphi_1}{\partial x^2} + \mu_{33}\frac{\partial^2\psi_1}{\partial z^2} + d_{33}\frac{\partial^2\varphi_1}{\partial z^2} + q_{311}\frac{\partial^2 W_1}{\partial x^2} = 0, \tag{67}$$

N_x' is expressed as follows:

$$N_x' = be_{311}V_0 + bq_{311}\Omega_0 + N_x^T. \tag{68}$$

Table 1. Properties of $BiTiO_3$-$CoFe_2O_4$ materials.

Properties	$BiTiO_3$-$CoFe_2O_4$
Elastic (Gpa)	$c_{11} = 226$, $c_{12} = 125$, $c_{13} = 124$, $c_{33} = 216$, $c_{44} = 44.2$
Piezoelectric (C/m)	$e_{31} = -2.2$, $e_{33} = 9.3$, $e_{15} = 5.8$
Dielectric (10^{-9} C/Vm)	$a_{11} = 5.64$, $a_{33} = 6.35$
Piezomagnetic (N/Am)	$q_{15} = 275$, $q_{13} = 290.1$, $q_{33} = 349.9$
Magneto-electric (10^{-12} Ns/VC)	$d_{11} = 5.367$, $d_{33} = 2737.5$
Magnetic (10^{-6} Ns^2/C^2)	$\mu_{11} = -297$, $\mu_{31} = 83.5$
Thermal moduli (10^5 N/Km^2)	$\beta_1 = 4.74$, $\beta_3 = 4.53$
Pyroelectric (10^{-6} C/N)	$p_3 = 25$
Pyromagnetic (10^{-6} N/AmK)	$\lambda_3 = 5.19$
Mass density (10^3 kg/m^3)	$\rho = 5.55$

In order to analysis the effect of external electrical voltage and magnetic potential on critical buckling temperature, the electrical potential difference V_0 and magnetic potential Ω_0 is applied to the upper and lower levels of the anisotropic nanobeam.

For clamped nanobeams subjected to constant voltage, the boundary condition is as follows:

$$W_1 \mid_{x=0,L} = 0, \left(\frac{\partial W_1}{\partial x}\right) \mid_{x=0,L} = 0, \left(\frac{\partial^3 W_1}{\partial x^3}\right)\Big|_{x=0,L.} = 0. \tag{69}$$

By considering eq. (65), the nanobeam deflection $W_1(x)$ can be computed. To determine the critical buckling temperatures of clamped nanobeams in eq. (65), by applying boundary condition and constant voltage and solving the eigenvalue problem, the amount of critical buckling temperatures is determined [41].

Also, for hingeded nanobeams subjected to constant magnetic potential, the boundary condition is as follows:

$$W_1 \mid_{x=0,L} = 0, \left(-Ig_{111111}\frac{\partial^4 W_1}{\partial x^4} + Ic_{1111}\frac{\partial^2 W_1}{\partial x^2} + Ag_{113113}\frac{\partial^2 W_1}{\partial x^2}\right)\Big|_{x=0,L} = 0, \left(\frac{\partial^2 W_1}{\partial x^2}\right)\Big|_{x=0,L} = 0. \tag{70}$$

As in the previous section, by applying boundary condition and constant magnetic potential and solving the eigenvalue problem, the amount of critical buckling temperatures of hinged anisotropic nanobeam is determined.

Results and discussion

This section addresses the thermal buckling of piezoelectric and piezomagnetic nanobeams. First, in order to investigate the accuracy of the developed equations, the results of the present paper are compared with those of other studies. Afterwards, the effect of different parameters on critical buckling temperature is demonstrated.

Table 1 presents the material properties of the $BiTiO_3$-$CoFe_2O_4$ in the nanobeams [36].

The higher-order elastic material properties must be determined through laboratory methods or molecular dynamics simulation. At present, there is scant research available on this subject. For elastic crystal centrosymmetric dielectric isotropy materials, higher-order constants are computed using $g_{111111} = c_{1111}l^2$, $g_{113113} = c_{1313}l^2$ relationships [42–46], where l is the size scale parameter. Piezoelectric materials are commonly central asymmetric materials. For 4 mm symmetry piezoelectric materials, higher-order constant coefficient are approximately considered according to the forgoing equations, and, the higher-order electro-mechanical coupling coefficient is considered $f = 5\,\mathrm{pCm^{-1}}$ according to laboratory results, [44–46]. Nanobeam length and thickness are assumed to be $L = (100\,\mathrm{nm})$ and $h = (5\,\mathrm{nm})$. In addition, the temperature difference of the nanobeam ends from the reference temperature T_0 is assumed to be $T_l - T_0 = 5\,\mathrm{K}$ [47].

Validation of results

In order to validate the results, considering that the thermal buckling of the elastic electromagnetic nanobeam is being investigated for the first time using the modified couple stress theory, the results obtained through the classical continuum theory are compared with those of refs. [47,48], as shown in tables 2 and 3. As is visible, the results obtained have good consistency with those of refs. [47,48].

Table 2. Comparing critical buckling temperatures of hinged and clamped nanobeams with uniform temperature variation for different L/h values.

(L/h)	Clamped ref. [48]	Present	Simply support ref. [48]	Present
10	1426.67	1430.38	354.16	357.5
20	354.2	357.59	90.09	89.4
30	166.7	165.35	42.14	41.33
40	90.22	89.4	22.55	22.34

Table 3. Comparing critical buckling temperatures of clamped nanobeam with uniform temperature rise ($L = 0.25\,\mathrm{m}$, $h = 0.01\,\mathrm{m}$).

Ref. [47]	Present
228.860	228.8604
711.323	711.3228

Table 4. Comparing nondimensional critical buckling temperatures ($\frac{T_{cr}}{I/\alpha AL^2}$) of hinged isotropic nanobeam with uniform temperature rise ($L/h = 5$).

Ref. [49] $l = 0$	Present, $l = 0$	$l = 0.01$	$l = 0.25$	$l = 0.5$	$l = 0.75$	$l = 1$	$l = 1.5$	$l = 2$	$l = 2.5$	$l = 3$
35.54	35.53	35.64	36.96	37.97	40.59	44.57	52.14	57.09	61.71	70.95

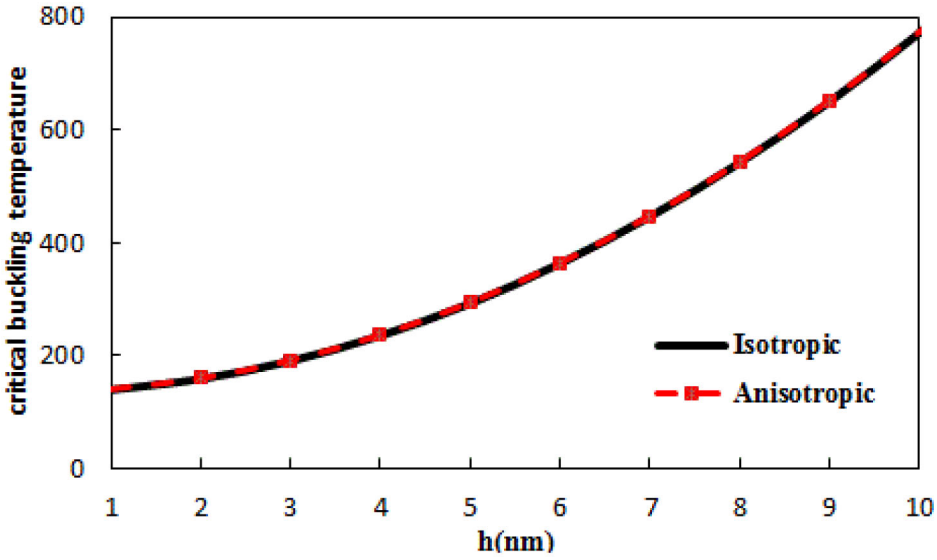

Fig. 2. Critical buckling temperatures of hinged isotropic and anisotropic nanobeams with uniform temperature rise for different values of thickness.

Another comparison study is carried out in table 4. As is clear, the results obtained based on the classical continuum theory ($l = 0$) have appropriate precision; besides, the results obtained through the modified couple stress theory ($l > 0$) are higher than those gained through the classical continuum theory which is in accordance with the literature. Consequently, tables 2–4 show the accuracy of the current study and interestingly, this model is able to accurately predict the buckling response of nanobeam.

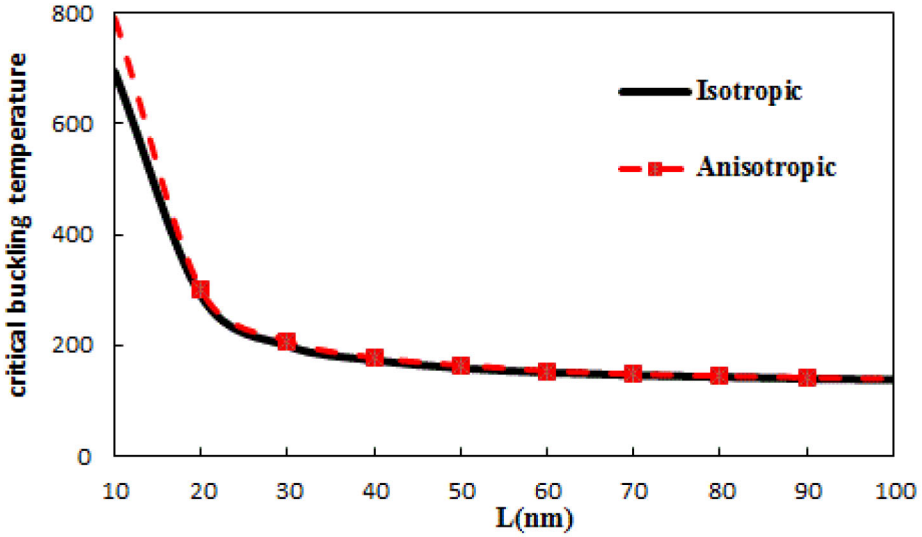

Fig. 3. Critical buckling temperature of hinged isotropic and anisotropic nanobeams with uniform temperature rise for different values of length.

Effect of thickness on critical buckling temperature

Figure 2 presents the critical buckling temperature variation of the hinged isotropic and anisotropic nanobeams for different values of thickness (h). Uniform temperature rise has been taken into account, the nanobeam length parameter is considered constant, and the assumption $l = 3\,\text{nm}$ has been made. As can be seen, the two diagrams follow a similar trend, *i.e.* an increase in thickness leads to an increase in the critical buckling temperature in isotropic and anisotropic nanobeam. As thickness increases, the nanobeam becomes thicker and, hence, stiffer, and the critical buckling temperature is increased.

In fact, a decrease in the nanobeam thickness increases the length-to-thickness ratio and causes the thinner nanobeam, which is more susceptible, to be unstable at lower temperatures.

In order to have deep insight on the influence of thickness parameter on critical buckling temperature, table 5 is presented for isotropic and anisotropic nanobeams for different thickness values. Accordingly, the difference between the critical buckling temperatures of isotropic and anisotropic nanobeams is infinitesimal.

Effect of length on critical buckling temperature

Table 5. Critical buckling temperature of hinged nanobeam with uniform temperature rise for different values of thickness ($L = 100\,\text{nm}$, $l = 3\,\text{nm}$).

h (nm)	1	2	3	4	5	6	7	8	9	10
Critical buckling temperature (K) Isotropic	139.7	159.14	190.76	235.66	292.7	363.1	446.22	541.88	649.51	771.54
Critical buckling temperature (K) Anisotropic	141.28	160.42	192.34	237.02	294.47	364.7	447.65	543.41	651.93	773.11

Figure 3 illustrates the effect of length parameter on critical buckling temperature of isotropic and anisotropic nanobeams with hinged boundary conditions. Uniform temperature rise is considered, nanobeam thickness is assumed to be constant, and the assumption $l = 3\,\text{nm}$ is made. As illustrated, the diagrams follow a similar trend, *i.e.* an increase in the length parameter leads to a decrease in the nanobeam stiffness and, consequently, decreases the critical buckling temperature of isotropic and anisotropic nanobeams; this effect is stronger on the anisotropic beam, though.

In order to carry out an accurate investigation, the critical buckling temperatures of the isotropic and anisotropic nanobeams for different values of the length parameter are presented in table 6.

As the nanobeam length parameter increases, the difference between the critical buckling temperature of isotropic and anisotropic nanobeams decreases, such that in lengths over 100 nm, no difference can be detected between two diagrams.

Table 6. Critical buckling temperature of hinged isotropic and anisotropic nanobeam with uniform temperature rise for different values of length ($h = 5\,\text{nm}$, $l = 3\,\text{nm}$).

L (nm)	10	20	30	40	50	60	70	80	90	100
Critical buckling temperature (K) Isotropic	701.1	287.2	199.6	172.18	159.24	151.2	146.69	143.64	141.16	140.15
Critical buckling temperature (K) Anisotropic	780.6	298.7	208.11	178.41	164.04	154.56	148.86	145.3	142.7	141.06

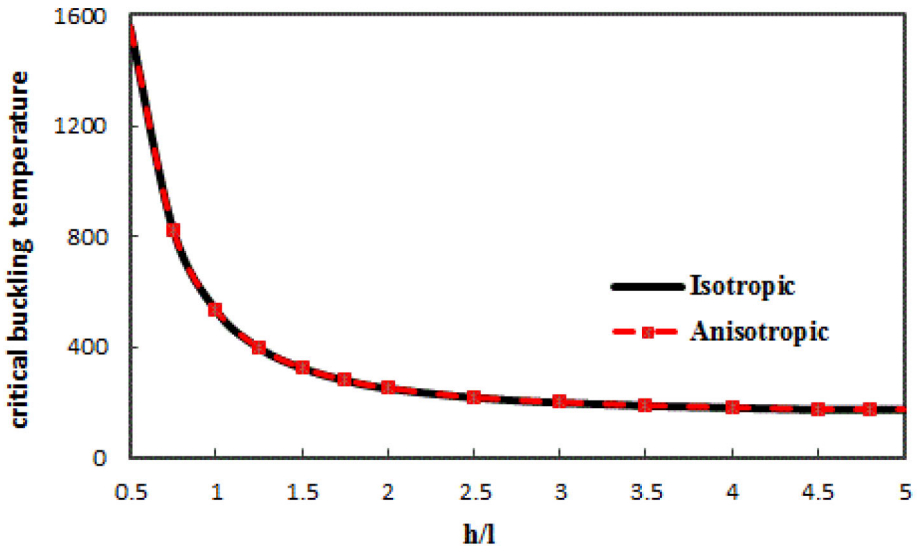

Fig. 4. Critical buckling temperature of hinged isotropic and anisotropic nanobeams with uniform temperature rise for different h/l values.

Table 7. Critical buckling temperature of hinged nanobeam with uniform temperature rise for different h/l values ($L = 100\,\text{nm}$, $h = 5\,\text{nm}$).

h/l	0.5	1	1.5	2	2.5	3	3.5	4	4.5
Critical buckling temperature (K) Isotropic	1556.1	824.82	532.21	397.49	324.24	280.05	251.48	218.13	199.51
Critical buckling temperature (K) Anisotropic	1557.7	825.81	534.36	399.39	326.7	281.92	253.27	219.59	201.33

Effect of dimensionless length scale parameter on critical buckling temperature

Figure 4 illustrates the effect of length scale parameter on the critical buckling temperature of isotropic and anisotropic piezoelectric and piezomagnetic nanobeams. Uniform temperature rise is considered, and nanobeam length and thickness are assumed to be constant ($L = 100$, $h = 5$). According to the illustration, the increase in the dimensionless length scale parameter (h/l), which is equivalent to a decrease in length scale parameter, leads to a decrease in the critical buckling temperature of isotropic and anisotropic nanotubes. In fact, as the length scale parameter decreases, nanobeam rigidity decreases, and consequently the critical buckling temperature decreases.

As illustrated, as the dimensionless length scale parameter increases, the results obtained from the modified couple stress theory approach to those obtained from the classical continuum theory, which shows the ability of the classical continuum theory to predict the buckling response of large-scale structures.

Table 7 presents the effect of the dimensionless length scale parameter on the critical buckling temperature of isotropic and anisotropic piezoelectric and piezomagnetic nanobeams obviously. According to the results, as the length scale parameter decreases, the critical buckling temperature of isotropic and anisotropic nanobeams decreases, too. Given the fact that the thermal expansion coefficient is considered identical for the isotropic and anisotropic electromagnetic nanobeams, it exerts no effect on the difference between the critical buckling temperatures of the two nanobeams, and there is no considerable difference in critical buckling temperature.

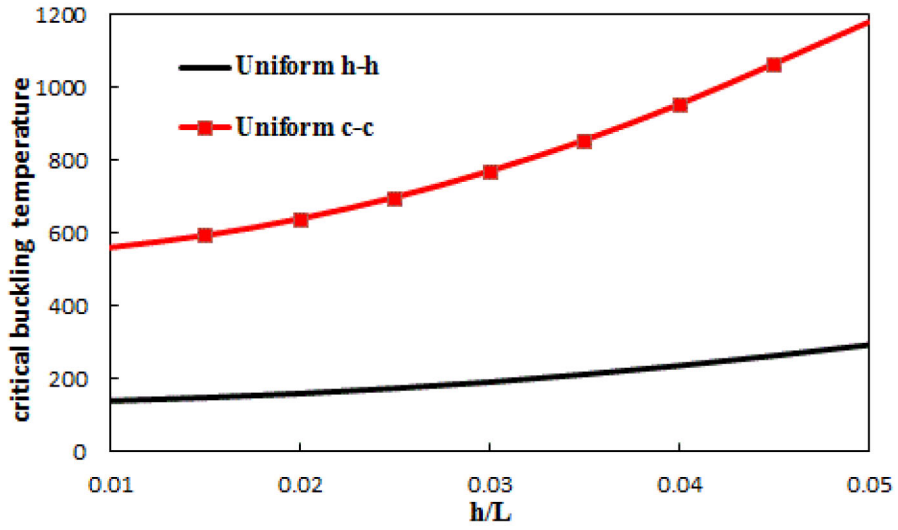

Fig. 5. Critical buckling temperature of hinged and clamped isotropic nanobeams with uniform temperature rise for different (h/L) values.

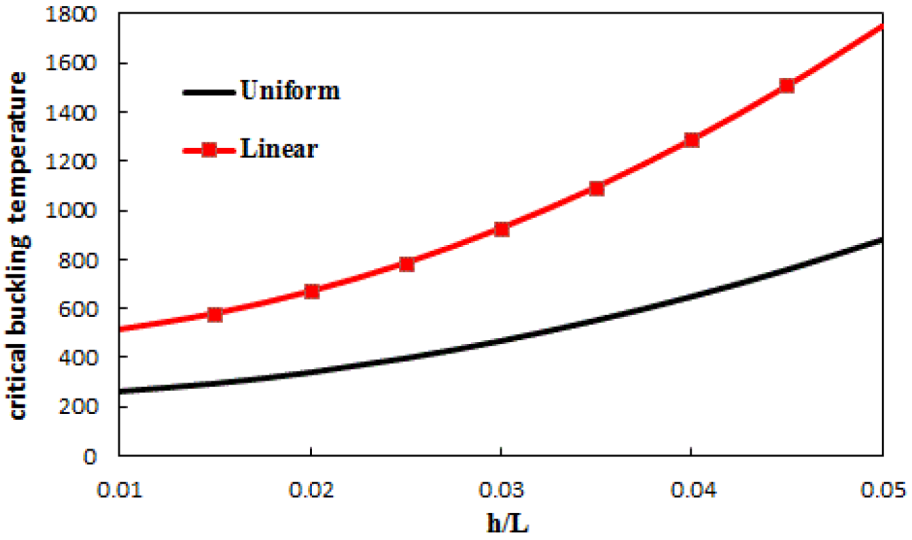

Fig. 6. Critical buckling temperature of clamped isotropic nanobeams with uniform, linear temperature rise for different h/L values.

Effect of boundary conditions on critical buckling temperature

Figure 5 presents the effect of boundary conditions on the critical buckling temperature of isotropic piezoelectric and piezomagnetic nanobeams for different nanobeam thickness-to-length ratios (h/L) and $l = 3\,\text{nm}$.

The diagram has been drawn for hinged and clamped boundary conditions, and temperature variation is assumed to be uniformed. As illustrated, due to the higher stiffness of clamped nanobeams as compared with hinged ones, the critical buckling temperature attains larger values in the clamped boundary condition in all thickness-to-length ratios. Besides, an increase in the thickness-to-length parameter leads to an increase in the effect of boundary conditions on the critical buckling temperature.

Effect of types of temperature rise on critical buckling temperature

Figure 6 presents critical buckling temperature variation of the isotropic clamped electromagnetic nanobeam with uniform and linear temperature variation for different nanobeam thickness-to-length rations (h/L) and $l = 2\,\text{nm}$.

As illustrated, the two diagrams follow a similar trend, in which, on the assumption of constancy of the length parameter, increase in thickness is accompanied by increase in critical buckling temperature. On the assumption of uniform temperature rise, temperature variation at all nanobeam points is identical, whereas temperature varies along nanobeam thickness in linear rise. Therefore, as thickness increases, increase in critical buckling temperature in linear temperature rise is higher than that in uniform temperature rise.

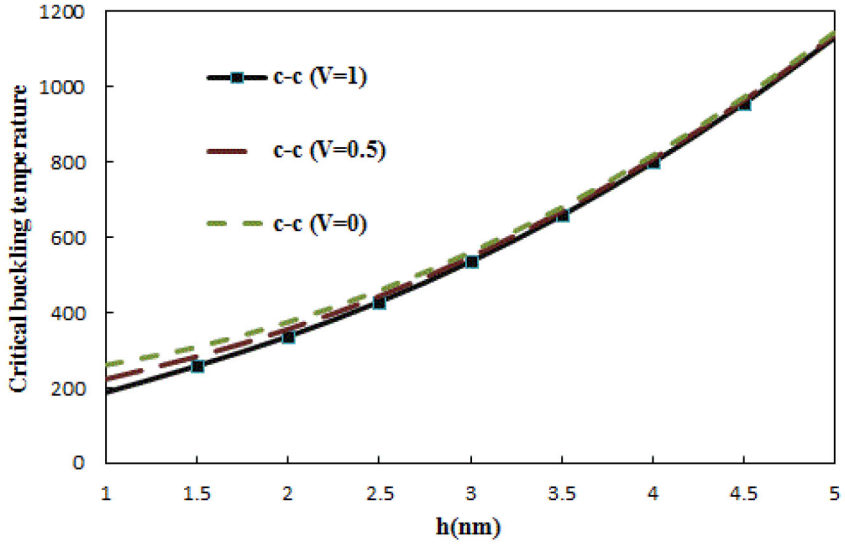

Fig. 7. Critical buckling temperature of clamped anisotropic nanobeam with uniform temperature rise for different value of electrical voltage.

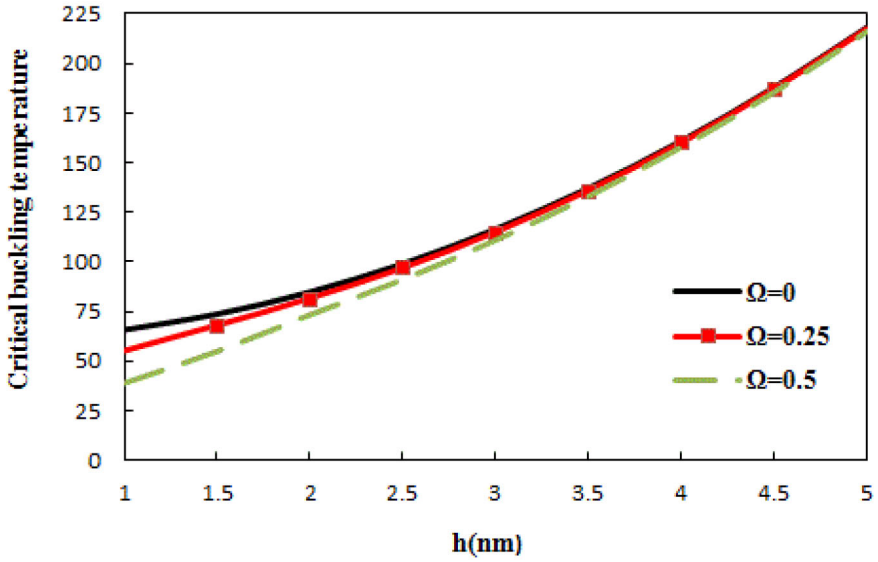

Fig. 8. Critical buckling temperature of hinged anisotropic nanobeam with uniform temperature rise for different values of magnetic potential.

Effect of external electric voltage and magnetic potential on critical buckling temperature

Figure 7 presents the critical buckling temperature variation of the clamped anisotropic nanobeams for different values of external electric voltage. The assumption $l = 2\,\text{nm}$ has been made. Uniform temperature rise is considered and nanobeam length is assumed to be constant. According to fig. 7, as the nanobeam thickness parameter increases, the difference between the critical buckling temperature of nanobeams decreases for different external electric voltage. Additionally, fig. 8 represents the critical buckling temperature variation of the hinged anisotropic nanobeams for different values of magnetic potential. According to fig. 8, the trend of critical buckling temperature changes with respected to thickness parameter is the same as fig. 7; such that as the thickness parameter decreases, the deference between critical buckling temperatures of nanobeam increase extremely for different values of magnetic potential. As illustrated, the positive electric voltage and positive magnetic potential decreases the critical buckling temperature. The reason is that compressive in plane force is generated in the nanobeams by imposing positive voltage and positive magnetic potential.

Table 8. Critical buckling temperature of clamped anisotropic nanobeam with uniform temperature rise for different values of electrical voltage.

h (nm)	$h=1$	$h=1.5$	$h=2$	$h=2.5$	$h=3$	$h=3.5$	$h=4$	$h=4.5$	$h=5$
Stability equations ($V=0$)	261.16	308.59	374.86	458.75	560.47	679.76	817.56	973.45	1146.97
Analytical method ($V=0$)	261.07	308.37	374.40	458.67	560.28	679.59	817.50	973.07	1146.56
Stability equations ($V=0.5$)	223.62	283.64	356.19	443.83	548.63	669.06	808.37	965.05	1139.28
Analytical method ($V=0.5$)	223.24	283.41	356.03	443.71	548.19	668.89	808.16	964.87	1138.96

Table 9. Critical buckling temperature of hinged anisotropic nanobeam with uniform temperature rise for different values of magnetic potential.

h (nm)	$h=1$	$h=1.5$	$h=2$	$h=2.5$	$h=3$	$h=3.5$	$h=4$	$h=4.5$	$h=5$
Stability equations ($\Omega=0$)	65.74	73.68	84.79	99.09	116.55	137.19	161.02	188.26	218.52
Analytical method ($\Omega=0$)	65.69	73.52	84.58	98.98	116.51	137.11	160.82	188.13	218.18
Stability equations ($\Omega=0.25$)	55.28	68.43	81.81	97.09	115.17	136.39	160.24	187.39	217.68
Analytical method ($\Omega=0.25$)	55.19	68.14	81.68	96.89	114.89	136.18	160.18	187.24	217.39

The critical buckling temperatures of the clamped and hinged anisotropic nanobeams for different values of the thickness parameter and different values of external electric voltage and magnetic potential are presented in tables 8 and 9, respectively. According to the results, the difference between the critical buckling temperatures of anisotropic clamped and hinged nanobeams for different solution method is infinitesimal.

Conclusion

In this paper, the thermal buckling of electromagnetic nanobeam was investigated on the basis of modified couple stress theory, which is capable to consider higher-order electro-mechanical coupling effect. The formulation was developed based on the Euler-Bernoulli beam model. The principle of minimum potential energy was utilized to develop the governing equations and boundary conditions. The thermal buckling of the nanobeam was investigated under two types of temperature rise and on the assumption of hinged and clamped boundary conditions. Besides, the equation was investigated in a semi-analytic fashion using the Galerkin method. The buckling behavior of isotropic and anisotropic nanobeams were studied as well. Finally, the following results were obtained:

1) By increase in thickness parameter which increases the nanobeam stiffness, the critical buckling temperature increase; while the influence of length parameter is in the opposite way; as such increase in length parameter leads to decrease in nanobeam stiffness.
2) The critical buckling temperature of the isotropic nanobeam is obtained lower than that of the anisotropic ones.
3) The increase in length scale parameter increases the nanobeam stiffness; also it is accompanied by increase in critical buckling temperature.
4) The boundary conditions have significant effect on the critical buckling temperature; as such, because clamped boundary conditions with respect to simply supported boundary conditions increases the stiffness of nanobeams, the critical buckling temperature increases, too.
5) The critical buckling temperature of the clamped nanobeam with uniform temperature rise is lower than that with linear temperature variation.
6) Due to generating compressive in plane force in the nanobeams, the imposing positive voltage and positive magnetic potential, reduce the critical buckling temperature.

References

1. C.W. Nan, Phys. Rev. B **50**, 6082 (1994).
2. S. Razavi, A. Shooshtari, Compos. Struct. **119**, 377 (2015).
3. C. Liu, L.L. Ke, Y.S. Wang, J. Yang, S. Kitipornchai, Compos. Struct. **106**, 167 (2013).
4. F. Ebrahimi, E. Salari, Smart Mater. Struct. **24**, 125007 (2015).
5. F. Ebrahimi, A. Rastgo, Thin-Walled Struct. **46**, 1402 (2008).
6. A. Kumaravel, J. Jones Praveen, R. Sethuraman, A. Arockiarajan, Appl. Mech. Mater. **592**, 2071 (2014).
7. S. Xu, Y. Shi, S.G. Kim, Nanotechnology **17**, 4497 (2006).
8. F. Mehralian, Y.T. Beni, R. Ansari, Int. J. Mech. Sci. **119**, 155 (2016).
9. N. Ebrahimi, Y.T. Beni, Steel Compos. Struct. **22**, 1301 (2016).
10. F. Mehralian, Y.T. Beni, R. Ansari, Compos. Struct. **152**, 45 (2016).
11. H. Razavi, A.F. Babadi, Y.T. Beni, Compos. Struct. **160**, 1299 (2017).
12. S.F. Dehkordi, Y.T. Beni, Int. J. Mech. Sci. **128**, 125 (2017).
13. F. Mehralian, Y.T. Beni, J. Braz. Soc. Mech. Sci. Eng. **40**, 27 (2018).
14. R. Ansari, H. Rouhi, S. Sahmani, Physica E **44**, 373 (2011).
15. A. Daneshmehr, A. Rajabpoor, A. Hadi, Int. J. Eng. Sci. **95**, 23 (2015).
16. L.L. Ke, Y.S. Wang, Smart Mater. Struct. **21**, 025018 (2012).
17. Y.T. Beni, M. Abadyan, A. Koochi, Phys. Scr. **84**, 065801 (2011).
18. H. Zeighampour, Y.T. Beni, F. Mehralian, Acta Mech. **226**, 2607 (2015).
19. H. Zeighampour, Y.T. Beni, Arch. Appl. Mech. **89**, 539 (2015).
20. F. Kheibari, Y.T. Beni, Mater. Des. **114**, 572 (2017).
21. R. Omidian, Y.T. Beni, F. Mehralian, Eur. Phys. J. Plus **132**, 481 (2017).
22. R.A. Toupin, Arch. Ration. Mech. Anal. **11**, 385 (1962).
23. R.D. Mindlin, H.F. Tiersten, Arch. Ration. Mech. Anal. **11**, 415 (1962).
24. W.T. Koiter, Proc. K. Ned. Akad. Wet. **67**, 17 (1964).
25. Y.T. Beni, I. Karimipöur, M. Abadyan, J. Mech. Sci. Technol. **28**, 3749 (2014).
26. A. Anthoine, Int. J. Solids Struct. **37**, 1003 (2000).
27. M. Mohammad-Abadi, A.R. Daneshmehr, Int. J. Eng. Sci. **74**, 1 (2014).
28. S.K. Park, X.L. Gao, J. Micromech. Microeng. **16**, 2355 (2006).
29. J.N. Reddy, J. Mech. Phys. Solids **59**, 2382 (2011).
30. Z. Belabed, M.S.A. Houari, A. Tounsi, S.R. Mahmoud, O.A. Bég, Composites Part B: Eng. **60**, 274 (2014).
31. Y.T. Beni, J. Mech. **33**, 289 (2017).
32. Y. Tadi Beni, J. Intell. Mater. Syst. Struct. **27**, 2199 (2016).
33. A. Nateghi, M. Salamat-talab, Compos. Struct. **96**, 97 (2013).
34. B. Akgöz, Ö. Civalek, Int. J. Eng. Sci. **85**, 90 (2014).
35. L.L. Ke, Y.S. Wang, Physica E **63**, 52 (2014).
36. L. Xu, S. Shen, Int. J. Appl. Mech. **5**, 1350015 (2013).
37. Y.T. Beni, Mech. Res. Commun. **75**, 67 (2016).
38. Y. Ootao, Y. Tanigawa, Compos. Struct. **68**, 471 (2005).
39. A.A. Khdeir, Acta Mech. **149**, 201 (2001).
40. F. Mehralian, Y.T. Beni, J. Mech. Sci. Technol. **31**, 1773 (2017).
41. M.A.A. Meziane, H.H. Abdelaziz, A. Tounsi, J. Sandwich Struct. Mater. **16**, 293 (2014).
42. F.A.C.M. Yang, A.C.M. Chong, D.C.C. Lam, P. Tong, Int. J. Solids Struct. **39**, 2731 (2002).
43. D.C. Lam, F. Yang, A.C.M. Chong, J. Wang, P. Tong, J. Mech. Phys. Solids **51**, 1477 (2003).
44. X.F. Li, B.L. Wang, K.Y. Lee, J. Appl. Phys. **105**, 074306 (2009).
45. K.A. Lazopoulos, A.K. Lazopoulos, Eur. J. Mech. A/Solids **29**, 837 (2010).
46. L.E. Cross, J. Mater. Sci. **41**, 53 (2006).
47. Y. Kiani, S. Taheri, M.R. Eslami, J. Therm. Stresses **34**, 835 (2011).
48. Y. Kiani, M.R. Eslami, Int. J. Mech. Mater. Des. **6**, 229 (2010).
49. A. Tounsi, A. Semmah, A.A. Bousahla, J. Nanomech. Micromech. **3**, 37 (2013).